

Near-Infrared Polarimetry of the Eagle Nebula (M16)

Koji SUGITANI,¹ Makoto WATANABE,² Motohide TAMURA,³ Ryo KANDORI,³ J. H. HOUGH,⁴
 Shogo NISHIYAMA,³ Yasushi NAKAJIMA,³ Nobuhiko KUSAKABE,⁵ Jun HASHIMOTO,^{1,6}

Takahiro NAGAYAMA,⁷ Chie NAGASHIMA,⁸ Daisuke KATO,⁸ and Naoya FUKUDA⁹

¹*Graduate School of Natural Sciences, Nagoya City University, Mizuho-ku, Nagoya 467-8501*

²*Subaru Telescope, National Astronomical Observatory of Japan, Hilo, HI 96720, USA*

³*National Astronomical Observatory of Japan, 2-21-1 Osawa, Mitaka, Tokyo 181-8588*

⁴*Center for Astrophysics Research, University of Hertfordshire, Hatfield, Herts AL10 9AB, UK*

⁵*Graduate University of Advanced Science, 2-21-1 Osawa, Mitaka, Tokyo 181-8588*

⁶*Department of Astrophysics, Tokyo University of Science, Shinjuku-ku, Tokyo 162-8601*

⁷*Department of Astrophysics, Kyoto University, Sakyo-ku, Kyoto 606-8502*

⁸*Department of Astrophysics, Nagoya University, Nagoya 464-8602*

⁹*Department of Computer Simulation, Okayama University of Science, Okayama 700-0005*

(Received 2007 January 12; accepted 2007 March 19)

Abstract

We carried out deep and wide ($\sim 8' \times 8'$) *JHKs* imaging polarimetry in the southern region of the Eagle Nebula (M16). The polarization intensity map reveals that two YSOs with near-IR reflection nebulae are located at the tips of two famous molecular pillars (Pillars 1 and 2) facing toward the exciting stars of M16. The centrosymmetric polarization pattern are consistent with those around class I objects having circumstellar envelopes, confirming that star formation is now taking place at the two tips of the pillars under the influence of UV radiation from the exciting stars. Polarization measurements of point sources show that magnetic fields are aligned along some of the pillars but in a direction that is quite different to the global structure in M16.

Key words: circumstellar — infrared: stars — ISM: individual (M16) — polarization — stars: formation

1. Introduction

Recent analyses of meteorites confirmed the presence of Fe isotopes of supernova origin in the early solar nebula and suggested that the solar system was formed in a massive star forming region (Tachibana & Huss 2003; Tachibana et al. 2006). Hester et al. (2004) and Hester & Desch (2005) presented a formation scenario of the sun-like low-mass stars and their planetary systems in massive star forming regions. The M16 region is important as it is a site with such an environment.

The Eagle Nebula (M16) is one of the most noticeable star forming regions following a comprehensive study of the three molecular gas pillars (Pillars 1 – 3) with HST (Hester et al. 1996). Near-infrared studies revealed that the protostar-like or very young objects M16ES-1 and M16ES-2 (Thompson et al. 2002), which were also identified as P1 and T1 by Sugitani et al. (2002) and as YSO-1 and YSO-2 by McCaughrean & Andersen (2002), are located at the tips of Pillars 1 and 2, respectively, facing toward the main exciting star of M16. Sugitani et al. (2002) reported that the locations of these young stellar objects and the elongated structures of the pillars suggested their formation as being due to the interaction with UV light from the OB stars in the NGC 6611 cluster, in analogy with the sequential star formation in some bright-rimmed clouds (Sugitani et al. 1995). Fukuda et al. (2002) used in-

terferometric observations of ^{13}CO and C^{18}O ($J = 1 - 0$), and of 2.7 mm continuum to indicate the propagation of star formation activity in the heads of these two pillars due to radiation or wind from the main exciting star. Healy et al. (2004) stated that the water masers in M16 were concentrated in the compressed gas layers within a few tenths of a parsec of the ionization front in three molecular pillars, one of which is Pillar 2, suggesting triggered star formation in their tip regions. Hester et al. (2004) also discussed the sequential nature of star formation in the pillars. For Pillar 3, Thompson et al. (2002) implied that the bright stars M16S-1 and M16S-2, which are located at the tip, were the results of recent star formation at the pillar head.

Thompson et al. (2002) estimated the luminosity of M16ES-1 and M16ES-2 to be $200 L_\odot$ and $20 L_\odot$, respectively, as a single object or a cluster of objects. They suggested that M16ES-1 is not a source of ionization radiation based on the absence of Pa α emission, and that it is either made up of multiple lower-luminosity objects or an object(s) in the earlier stage of ZAMS, i.e., protostar stage. On the other hand, McCaughrean & Andersen (2002) estimated the extinction of M16ES-1 and M16ES-2 to be 27 and 15 mag., respectively, assuming their *J*s and *H* fluxes to be photospheric, and concluded that a $10 M_\odot$ ZAMS star and $2.5 M_\odot$ ZAMS star were located at the tips of Pillars 1 and 2, respectively. It is not clear, from

these observations, whether single stars of relatively high masses or multiple lower-mass stars have formed there. Thus, further observations are required to address this issue.

Recently, Miao et al. (2006) developed 3-D hydrodynamical model for the dynamical evolution of molecular clouds irradiated by UV light from massive stars, i.e., bright-rimmed clouds. They noted that since their model adequately included self-gravity and treated the chemical and thermal evolution, it had advantage in the detailed study of triggered star formation over previous 2-D/3-D models that did not fully include all of these effects (e.g., Bertoldi 1989; Lefloch & Lazareff 1994; White et al. 1999; Williams et al. 2001; Kessel-Deynet & Burkert 2003), although these models successfully reproduced some of the observed properties of bright-rimmed clouds. Miao et al. (2006) applied their model for Pillar 2 and suggested that the core of Pillar 2 is at a transition stage toward induced star formation due to the shock that precedes an ionization front moving toward the core. In fact, a water-maser source, which indicates an object in the very early stage of stellar evolution, is detected near the core of Pillar 2 (Pound 1998; White et al. 1999; Fukuda et al. 2002) a few arc-seconds inside of M16ES-2, which is located at the ionization front (Healy et al. 2004), suggesting further induced star formation in Pillar 2. However, these models do not predict magnetic field behavior in detail, although Miao et al. (2006) did include magnetic pressure and Bertoldi (1989) used an approximate expression for the magnetic flux. The lack of a full treatment of magnetic fields is due to the modeling complexity and to the paucity of observations of magnetic fields in and around molecular clouds associated with HII regions.

Orsatti et al. (2006) presented polarimetric *UBVRI* observation data of NGC 6611, including those of Orsatti et al. (2000). They identified the presence of nearby dust clouds located on the Local arm that have slightly a larger mean λ_{\max} ¹ than that of the average interstellar medium. The mean position angle of the e-vectors was estimate to be $\sim 70^\circ$. However, these optical observations will only be relevant for stars with small extinction and hence will not provide information on the magnetic field deep within molecular clouds. Thus, infrared polarimetric observations are important.

We conducted deep, near-IR polarimetric observations in M16 to reveal the details of M16ES-1/2 and to obtain magnetic field structures in this region. We also aimed to search for more near-IR reflection nebula sources in this region. Here we present the results of our observations and discuss the details of M16ES-1/2 and the magnetic field behavior in this region. The polarimetry instrument used in this study is SIRPOL, which is the attachment of the SIRIUS camera mounted on the 1.4-m IRSF telescope at the South Africa Astronomical Observatory (SAAO). Its distinctive feature is presented in Kandori et al. (2006) and Tamura et al. (2007).

2. Observations and Data Reductions

In the southern region of M16 (figure 1), simultaneous *JHKs* polarimetric observations were carried out using the SIRIUS camera and its attachment polarimeter mounted on the 1.4-m IRSF telescope at SAAO. The SIRIUS camera is equipped with three 1024×1024 HgCdTe (Hawaii) arrays, *JHKs* filters, and dichroic mirrors, which enable simultaneous *JHKs* imaging. The field of view at each band is $\sim 7\farcm7 \times 7\farcm7$, with a pixel size of $0\farcs45$. The polarimeter is composed of an achromatic (0.5–2.5 μm) wave-plate rotator unit and a high-extinction-ratio polarizer, both of which are attached upstream of the camera and at room temperature. Details of the SIRIUS camera are presented in Nagashima et al. (1999) and Nagayama et al. (2003), and those of the polarimeter in Kandori et al. (2006).

The total exposure time was 900 s per wave-plate angle. We obtained 10 dithered exposures, each 10 s long, at 4 wave-plate angles (0° , 22.5° , 45° , and 67.5°) as one set of observation. We repeated this set 9 times. Sky images were also obtained in between target observations. The seeing during the observations was $1\farcs1$ (2.5 pixel) in the *Ks* band.

After the standard procedures for near-IR image reduction with IRAF (dark subtraction, flat-fielding with twilight-flats, bad-pixel substitution, sky subtraction, and averaging of dithered images), we evaluated the Stokes parameters (I , Q , U), the degree of polarization P , and the polarization angle θ as follows; $Q = I_0 - I_{45}$, $U = I_{22.5} - I_{67.5}$, $I = (I_0 + I_{45} + I_{22.5} + I_{67.5})/2$, $P = \sqrt{Q^2 + U^2}/I$ and $\theta = (1/2)\arctan(U/Q)$. The absolute accuracy of position angle of polarization was estimated to be better than 3° based on the measurements during the commissioning run. The polarization efficiency at *JHKs* were also estimated to be higher than 96% and, therefore, no correction of P was made here.

Aperture polarimetry was performed for point sources detected by DAOFIND in the field of view. The DAOPHOT package was used to evaluate the point source magnitudes for 4 wave-plate angles at *H* and *Ks*. The limiting magnitudes (at 0.1 mag error level) of each wave-plate angle are estimated to be 18.0 and 17.0 at *H*, and *Ks*, respectively. The 2MASS data were used for magnitude calibration. All the sources with photometric errors of ≥ 0.1 mag were rejected. The errors of the degree of polarization and position angle were calculated from the photometric errors, and the degrees of polarization were debiased (Wardle & Kronberg 1974).

3. Results and Discussion

3.1. Intensity and polarization images of the overall region

The *JHKs* intensities are shown as a composite color image in figure 1. In the central region of this image, the famous elephant trunks (Pillars 1–3) are identified as areas of lower stellar density, together with a molecular cloud that is at the base of the pillars (near HH 216).

¹ the wavelength of maximum interstellar polarization



Fig. 1. Three-color composite image of $JHKs$ intensities in M16. The $JHKs$ data are represented as blue, green, and red, respectively. The area of the image is $\sim 7'7 \times 7'7$. North is at the top, east to the left. The yellow color regions at the upper right corner and near the middle of the right edge are dead pixel regions of the J band array.

Toward the south-east region of the image, Pillar 4 and its neighboring molecular clouds (McCaughrean & Andersen 2001; Andersen et al. 2004) are also identified. Relatively strong extended nebular emission is seen around Pillars 1–3, and there is rim-brightening emission of the molecular cloud edges (Pillars 1–4, and a cloud near HH 216) facing the exciting stars that are located to the north-west, but out of this image. The rim-brightening emission seems to be reflection from the OB star light and/or from HII gas at the surfaces of the molecular clouds. The $JHKs$ polarized intensities (PI) are presented as a composite color image in figure 2, where PI is the product of P and I . Distinctive polarization emission nebulae are only identified toward the two YSOs M16ES-1 and M16ES-2. This suggests that most of the extended nebula emission and rim-brightening emission are not reflected light from the OB stars, but comes from HII gas continuum/line emission.

3.2. Intensity and polarization properties of YSOs at the tips of Pillars 1 and 2

3.2.1. M16ES-1

A polarization vector map toward M16ES-1 of Pillar 1 is shown superimposed both on the I and PI images at each band in figure 3. The appearance of the nebulae in the PI image is significantly different from that in the I image at each band. The polarized nebula emission is seen mostly around M16ES-1, while the nebula emission of the I image is seen both around M16ES-1 and at the rim region facing toward the exciting stars of M16. However, the polarization vector maps indicate weak polarized emission in the rim region, although it is not clearly recognized in



Fig. 2. Three-color composite image of polarized intensity in M16. The $JHKs$ data are represented as blue, green, and red, respectively. The area of the image is $\sim 7'7 \times 7'7$. North is at the top, east to the left. The blue color regions at the upper right corner and near the middle of the right edge are dead pixel regions of the J band array.

the PI images.

Strong polarized emission is asymmetrically distributed just north and south of M16ES-1 in the Ks and H bands, while point-like weak polarized emission is seen immediately north of M16ES-1 in the J band. The polarization vectors of the asymmetric emission clearly show a centrosymmetric pattern that is probably due to the illumination of M16ES-1, in the Ks and H bands, although this pattern is not clearly seen in the J band. These suggest that the polarized emission comes from the walls of two (north and south) cavity lobes, which were created by the bipolar outflow from M16ES-1 and are still embedded in the molecular gas. The north lobe has two (NW and NNE) sub-peaks/features and the south one also has two (SE and SSW) features in the PI images of Ks and H . The degrees of polarization of the south lobe are 20% or more, somewhat higher than those of the north lobe whereas the intensities are higher in the north lobe than in the south one.

It is possible that these four sub-peaks/features are bright regions within a single bipolar cavity lobe, although it is difficult to eliminate the possibility that the outflow system consists of two pairs of bipolar outflows. In the latter case, the NW and NNE features would be counterparts of the SE and SSW features, respectively, suggesting either a binary star system or the precession of a single bipolar outflow. Thompson et al. (2002) point out the possibility that M16ES-1 consists of multiple low luminosity objects and our results would appear to support this. However, the NW and NNE features might be coincident with the two 2.7 mm continuum peaks y and x of Fukuda

et al. (2002), respectively. If they are, then this would indicate that the feature are either free-free emission from ultra-compact HII regions, i.e., high-mass protostar hypothesis (McCaughrean & Andersen 2002), or that they are dust emission from very dense regions (Fukuda et al. 2002), which are located on top of the cavity with surfaces that strongly reflect the light from M16ES-1. The polarization vectors toward these two features seem to support the latter possibility. The H_2 image of Thompson et al. (2002) shows some emission corresponding to the NW and NNE features, which also supports the idea that the two 2.7 mm continuum peaks are dust emission, indicating dense cores that have enough masses to form low-mass stars. Higher resolution observations both at radio and infrared wavelengths, however, are required to reveal the detailed structures around M16ES-1.

A gap is clearly seen between the NW and SE features (around the center of the centrosymmetric vector pattern) in the *PI* images of the K_s and H bands. This is due to the very-low degree of polarization toward the gap region, since the intensities at the K_s and H bands are very high there. This gap most likely corresponds to a small disk-like structure (Sugitani et al. 2002), perpendicular to the axis of the cavity lobe(s), although the usual “polarization disk” (parallel polarization pattern; e.g., Warren-Smith et al. 1987) is not evident. This is most likely due to the modest spatial resolution of the observations, with a range of polarization position angles from the reflection nebulae producing a very small degree of polarization. If this is the case, a disk-like structure with a size of several thousand AU is expected (Whitney & Hartmann 1993; Fischer et al. 1994). Here the disk would appear to be tilted so that the north side is near to us, producing the higher polarized intensity of the north lobe and the higher degree of polarization of the south lobe.

Weak polarized emission is seen along the rim region in the polarization vector maps of the H and J bands, and the polarization vectors are nearly perpendicular to the direction of the exciting star(s) from the tip of Pillar 1. Thus, this polarized emission along the rim region is most likely to be reflected light from the OB stars of M16, but significantly weaker than that occurs in M42 (Tamura et al. 2006). The degree of polarization is slightly higher at the J band than at the H band, and no alignment of the polarized vectors is recognized at the K_s band. These may be due to dilution by line emission (e.g., H_2 , $Br\gamma$) from HII gas at longer wavelengths.

3.2.2. M16ES-2

A polarization vector map toward M16ES-2 of Pillar 2 is shown superimposed both on the I and *PI* images for each band in figure 4. The polarization vectors toward M16ES-2 clearly show a centrosymmetric pattern, which is probably due to illumination by M16ES-2, and a polarization disk is seen at the center of the centrosymmetric pattern. In the H band, the polarized emission is clearly more constricted to the east and west of the approximate center of the centrosymmetric pattern. Similar trends are also seen at J and K_s . These, together with the larger total and polarized intensities to the north, but larger de-

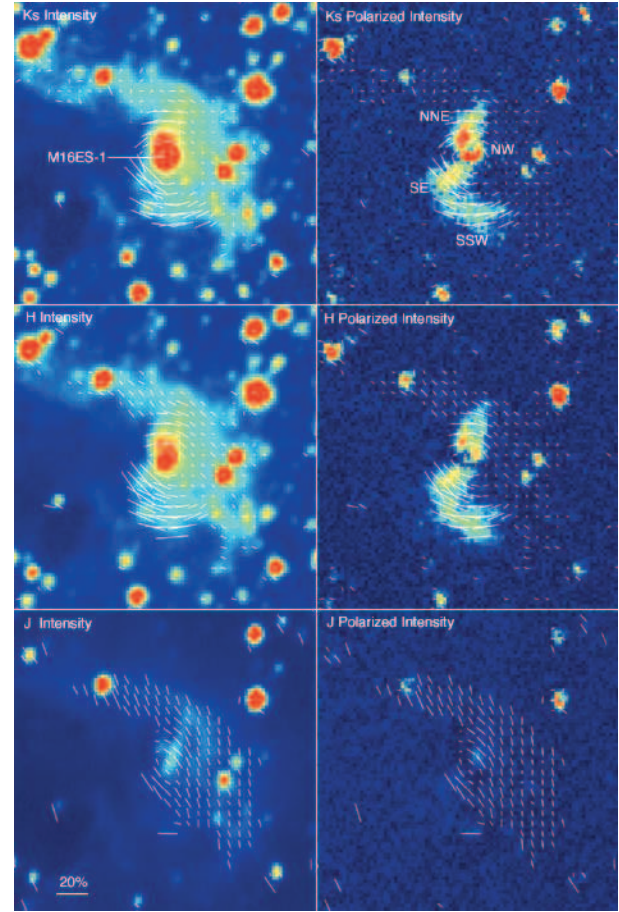


Fig. 3. JHK_s polarization vector maps superposed on the total and polarized intensity images of M16ES-1 located at the tip of Pillar 1. The area of the image is $40'' \times 40''$. North is at the top, east to the left. The main exciting star of M16 is located to the west-northwest.

grees of polarization to the south (except in the outermost regions) are all consistent with a disk-like structure with a size of a few thousand AU, which is significantly tilted so that the north side is near to us.

Sugitani et al. (2002) reported a dark lane in the middle of the M16ES-2 nebulosity, suggestive of an associated disk-like structure, and Thompson et al. (2002) also suggested that the surrounding nebulosity of M16ES-2 is double. McCaughrean & Andersen (2001) suggested that the double nature of the nebulosity is due to a faint second source $1''$ south of M16ES-2, which is a lightly reddened field star. In order to examine further the detailed morphology of the nebulosity, we checked the HST/NICMOS camera 2 archival images (Thompson et al. 2002). Figure 5 shows the NICMOS 2 infrared image of M16ES-2. The nebula extent in our total and polarized intensity maps appears consistent with that in the NICMOS 2 image. The NICMOS nebula peak is not located at the center of the centrosymmetric pattern or the constriction, but within the north nebula (figure 4 and 5). This offset is probably due to the tilt of the disk-like structure and the central source might not be seen directly. Although a faint

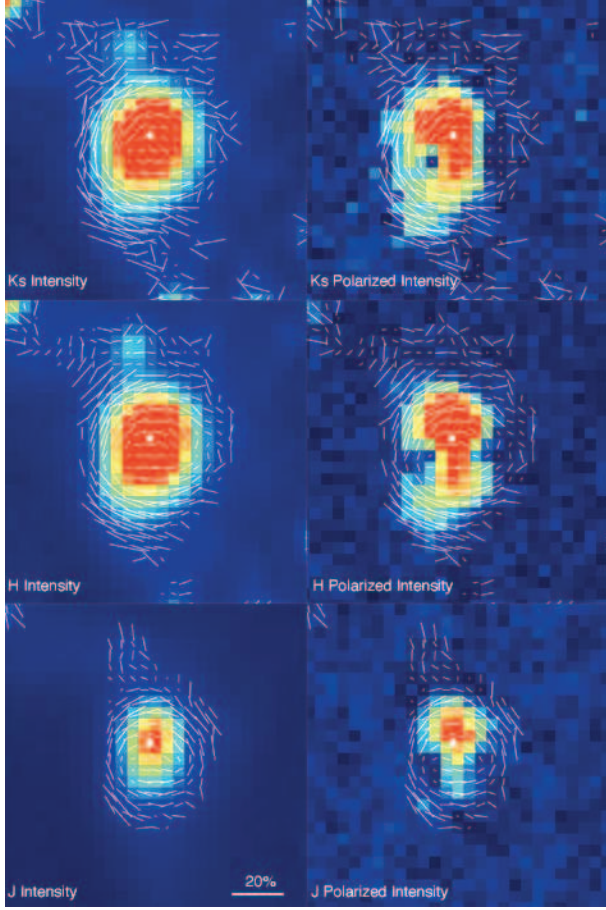


Fig. 4. $JHKs$ polarization vector maps superposed on the total and polarized intensity images of M16ES-2 located at the tip of Pillar 2. The area of the image is $12'' \times 12''$. North is at the top, east to the left. The approximate position of the nebula peak in the HST/NIC 2 image (figure 5) is marked by a white dot at each panel.

source $\sim 1\text{--}2''$ south of the center (M16ES-2) is identified, it is not the origin of the bipolar nebulosity with the intensity of the south nebula being much weaker than the north nebula.

We conclude that the bipolar nebula is mainly produced by scattered light from a central source obscured by a tilted disk-like structure.

3.3. Aperture Polarimetry and Magnetic Field Structures

3.3.1. Global magnetic field structure

Figure 6 shows the H band polarization vector map of point-like sources with aperture polarimetry. Only the sources detected both at H and Ks with photometric errors of < 0.1 mag and polarization angle errors of $< 15^\circ$ are included. The bright saturated and crowded sources, which could not be measured correctly, are rejected.

The polarization vectors are well aligned with each other, and therefore their polarizations are considered to be produced by dichroism arising from aligned grains in the cloud (e.g., Tamura et al. 1987). The general regular-

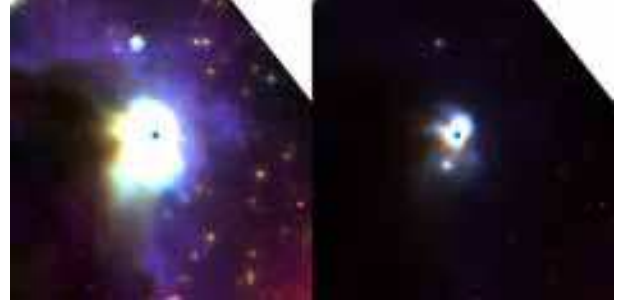


Fig. 5. Three-color composite image of F110W/F160W/F205W intensities toward the tip of Pillar 2. The F110W/F160W/F205W data obtained with HST/NIC 2 are represented as blue, green, and red, respectively. North is at the top, east to the left. Both images show the same area as that of figure 4 with a size of $12'' \times 12''$, but the scale of the right one is changed to show a constriction of the nebulosity, a faint star, and the difference of intensity between the north and south reflection nebulae.

ity of the position angles indicates a large-scale magnetic field over the observed area, with the polarization vectors representing the direction of the magnetic field.

The dominant field direction is $\theta \sim 80\text{--}90^\circ$ with a considerable spread as shown in figure 7 (*dashed lines*). A small difference in θ is observed between the H and Ks bands [figure 7(a) and figure 7(b), respectively]. The field direction in the north-east quadrant of the observed area is $\sim 70^\circ$ significantly different from those of the other three quadrants.

Orsatti et al. (2006) reported 70.0 ± 2.5 and 73.7 ± 2.5 as the mean polarization angles of the stars of the NGC 6611 cluster and its surroundings, respectively. Their values are somewhat smaller than our value of $\sim 80\text{--}90^\circ$, but their optical measurements will only sample stars at lower optical depths.

To further examine the magnetic field structures in the M16 dark clouds, we divide our sample into two groups (high and low reddened sources) using $H - Ks$ colors. According to Sugitani et al. (2002), there are two distinct source distributions divided at around $H - K \sim 0.6$ in the color-color ($J - H$ vs. $H - K$) diagram. Many of the highly reddened sources ($H - K \geq 0.6$) are background stars (dwarfs and giants) reddened by the M16 clouds, and many of those with low reddening ($H - K < 0.6$) are either foreground or stars at low optical depths within the M16 clouds. The polarization of stars at low reddening may well have a large contribution from interstellar polarization, produced in the front of the M16 clouds. The polarization of highly reddened stars will be produced mainly within the M16 clouds. Figure 7 shows the histograms of position angles of the observed polarizations for these strongly and weakly reddened sources (*solid* and *dot-dashed lines*, respectively). The highly reddened sources have a different mean θ of $\sim 90^\circ$ ($\overline{\theta_H} = 84^\circ \pm 22^\circ$ and $\overline{\theta_{Ks}} = 94^\circ \pm 28^\circ$) from those with low reddening ($\overline{\theta_H} = 102^\circ \pm 18^\circ$ and $\overline{\theta_{Ks}} = 110^\circ \pm 30^\circ$). The position angles in the H and Ks bands correlate well with each other (figure 8a), but differ by $\sim 10^\circ$ on the average [figure 8b;



Fig. 6. H band polarization vector map of point sources superposed on the H band intensity image. For sources of $H - Ks \geq 0.6$ their polarization vectors are shown by white bars, for source of $H - Ks < 0.6$ by green bars.

$$\overline{\theta_H - \theta_{Ks}} = -10^\circ \pm 30^\circ \text{ (for } H - Ks \geq 0.6\text{) and } -8^\circ \pm 36^\circ \text{ (for } H - Ks < 0.6\text{).}$$

Martin (1974) and Messinger et al. (1997) interpreted the wavelength dependence of position angles to the same sources as arising from two clouds along the line of sight, having different dust size distributions and different magnetic field directions. Toward M16, there may exist at least two types of dust clouds; one is the clouds associated with M16 and another the interstellar medium located on the Local arm. Figure 7 shows that the magnetic field direction in the M16 clouds is $\sim 90^\circ$, while θ of ~ 100 – 110° is suggested in the interstellar medium. A tendency for the position angle to be slightly larger at Ks than at H could be explained by the larger influence of the interstellar medium at longer wavelengths. The similar tendency is also seen for sources with smaller $H - Ks$ colors, probably because a number of sources reddened by the M16 clouds are still included in the smaller $H - Ks$ color sample. The optical polarization of sources in Orsatti et al. (2006) might be mostly dominated by the M16 clouds and their θ might be therefore smaller than ours. The larger influence of the interstellar medium at longer wavelengths may indicate a larger mean dust size in the interstellar medium than in the M16 clouds because a larger dust produces a larger polarization at infrared wavelengths. A larger dust size is consistent with the larger mean λ_{\max} in the nearby dust clouds located on the Local arm than in the M16 clouds that has λ_{\max} similar to the general interstellar medium (Orsatti et al. 2006). SIRPOL observations have shown wavelength dependent θ in other star forming regions and these will be studied in detail in the future.

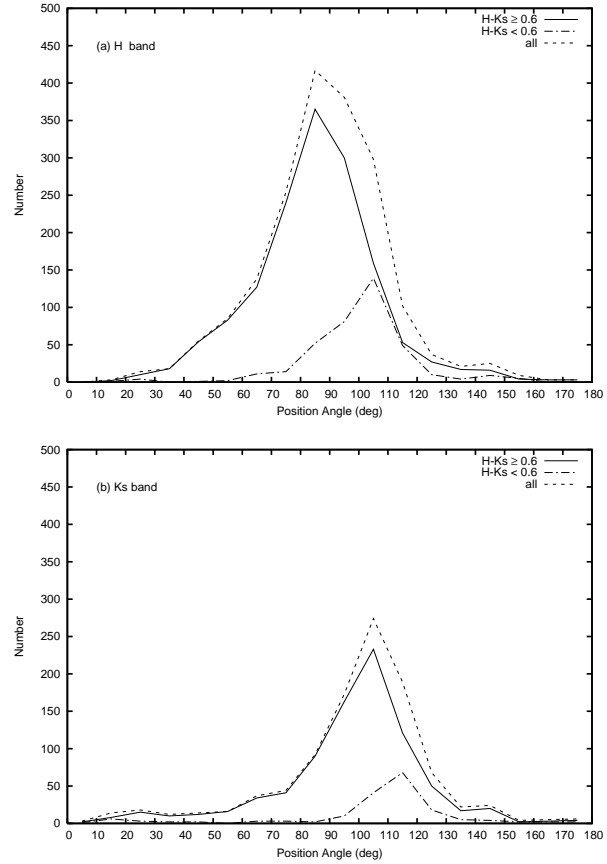


Fig. 7. Histograms of polarization angles of point sources in the H and Ks bands. Only sources are included that have photometric errors of ≤ 0.1 mag and polarization angle errors of $< 15^\circ$. The width of each bin is 10° .

3.3.2. Local magnetic field structures

As shown in figure 6, the north-east quadrant of the observed area has $\theta \sim 60$ – 70° , which is different from the global value of ~ 80 – 90° .

It is interesting to examine the magnetic field direction within the pillars. The field direction of Pillar 2 seems to be well aligned with the elongation axis of Pillar 2, but at quite a different angle to the rest of the cloud. A similar trend is also seen for Pillar 3. In order to examine the relationship in more detail, we list the position angles of the elongation axes of the Pillars, the magnetic field directions in and around them, and the directions to the Pillars of UV radiation from the main exciting star (HD 168076; O5 star) to them. The position angles of the Pillars were determined by eye, and the magnetic field directions by selecting sources within $30''$ of their axes, which covers most of the length of the pillars (figure 9). Only sources with $H - Ks \geq 0.6$ are included to eliminate foreground stars, which for Pillar 1 includ sources only toward its head (see figures 1 and 6).

The pillar axes are nearly aligned with the direction of the UV radiation from the main exciting star of M16 (table 1). This suggests that Pillars 1–3 might have been strongly affected by the UV radiation with their present

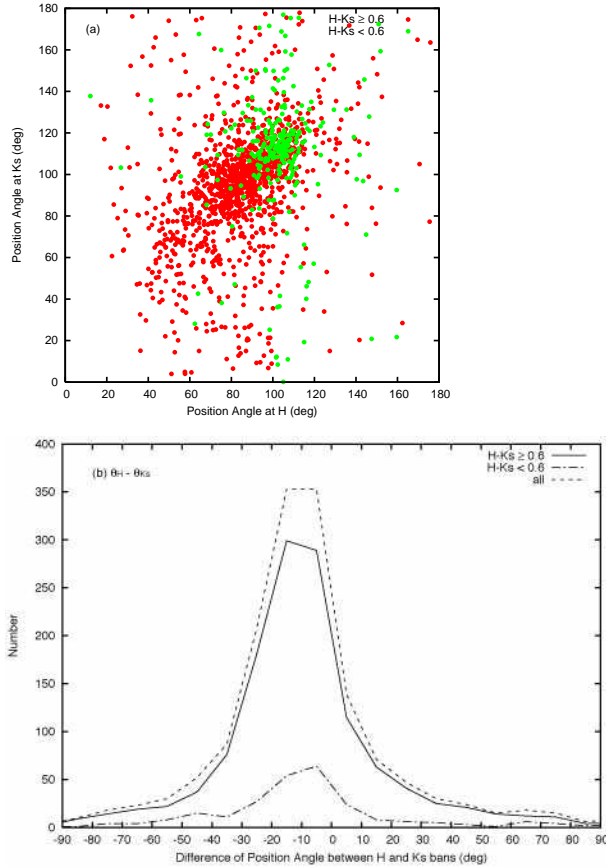


Fig. 8. (a) Correlation of polarization angles between the H and Ks bands (left) and (b) histogram of the difference of position angles between the H and Ks bands (right). Only sources are included that have photometric errors of ≤ 0.1 mag and polarization angle errors of $< 15^\circ$. The width of each bin of the histogram is 10° .

structures formed through this UV influence (White et al. 1999; Williams et al. 2001; Fukuda et al. 2002; Miao et al. 2006; Kessel-Deynet & Burkert 2003). This strong influence could cause increasing curvature of the clouds' rim, and the cloud magnetic field could be strongly dragged away from the direction of the main exciting star by the shock that precedes the ionization front, if the magnetic field is frozen into the gas (e.g., Bertoldi 1989), and then the direction of the field could be eventually aligned with the direction toward the exciting star, i.e., the pillar axis direction. The magnetic field direction of Pillar 2 is estimated to be $\sim 130^\circ$, and nearly the same as both the pillar axis and the UV incident direction of $\theta \sim 120\text{--}130^\circ$, while that of the ambient field differs from these θ by $\sim 30\text{--}40^\circ$. This difference is likely to be the results of the magnetic drag by the ionization/shock front in the formation of Pillar 2. For Pillar 1 and 3 a similarity is also seen with nearly the same directions for the magnetic field, pillar axes and UV radiation, although the numbers of polarization angles are very small. No clear difference is seen between Pillar 1 and the ambient field directions, as might be expected, because the direction of the UV

radiation is similar to that of the global magnetic field.

The ambient magnetic field directions of Pillars 1–3 are almost the same as that of the global field, suggesting the ambient field has not been disturbed. If these magnetic field directions are those of the initial magnetic field, the magnetic field strength could not be large enough to regulate the entire structures of the pillars and the ionization gas pressure could be dominant over the magnetic pressure in the formation of the pillar structures. However, we have to wait for a future 3-D hydrodynamical model that fully treats magnetic effects to know the detailed behavior of magnetic fields in and around the pillar.

At the tips of Pillar 1–3, signs of recent star formation have been reported and this study also suggests that M16ES-1/2 are in the early evolution stage of stellar objects. The magnetic field directions suggest the pillar structures are strongly influenced by the UV radiation. Thus, it is very likely that these YSOs were also formed under the influence of the ionization/shock fronts introduced by the UV radiation, although it is also possible that stars were naturally formed in dense cores and that then ionization/shock fronts come through the dense cores. However, YSOs were identified only toward the pillar tips. If stars form naturally in the pillars, some YSOs could be identified toward the pillar tails. The alignment between the pillar axes and the UV incident directions imply that the ionization/shock fronts made the entire pillar structures from the less dense natal clouds and, then, their substructures as shown by hydromagnetic models (e.g., Bertoldi 1989; Lefloch & Lazareff 1994; White et al. 1999; Williams et al. 2001; Kessel-Deynet & Burkert 2003). Particularly, Kessel-Deynet & Burkert (2003) imply that a radiatively impeded globule repeats leaving small cores decoupled from itself, which collapse after the passage of the ionization/shock fronts and form stars, i.e., sequential star formation in the globule. If this repeated process occur at the pillar tip, the sequential nature of star formation, such as mentioned in section 1, could be good evidence for induced star formation.

Thus, the magnetic fields along the pillar axes could indicate the strong influence with UV and could consequently provide the possibility of induced star formation together with star formation signs at the pillar tips/surfaces. However, since the sample number is very small at present, it is vitally necessary to increase the sample number to further know the general behavior and role of the magnetic field in the evolution and star formation of bright-rimmed clouds (pillars around HII regions).

4. Conclusion

We have conducted deep and wide ($\sim 7.7 \times 7.7$) $JHKs$ imaging polarimetry in the south region of M16. Main findings are summarized as follows.

1. The extended nebular emission around Pillars 1–3 is not reflection light of the OB stars of NGC 6611, but the continuum/line light of the HII region.
2. Strong reflection light can be detected only to

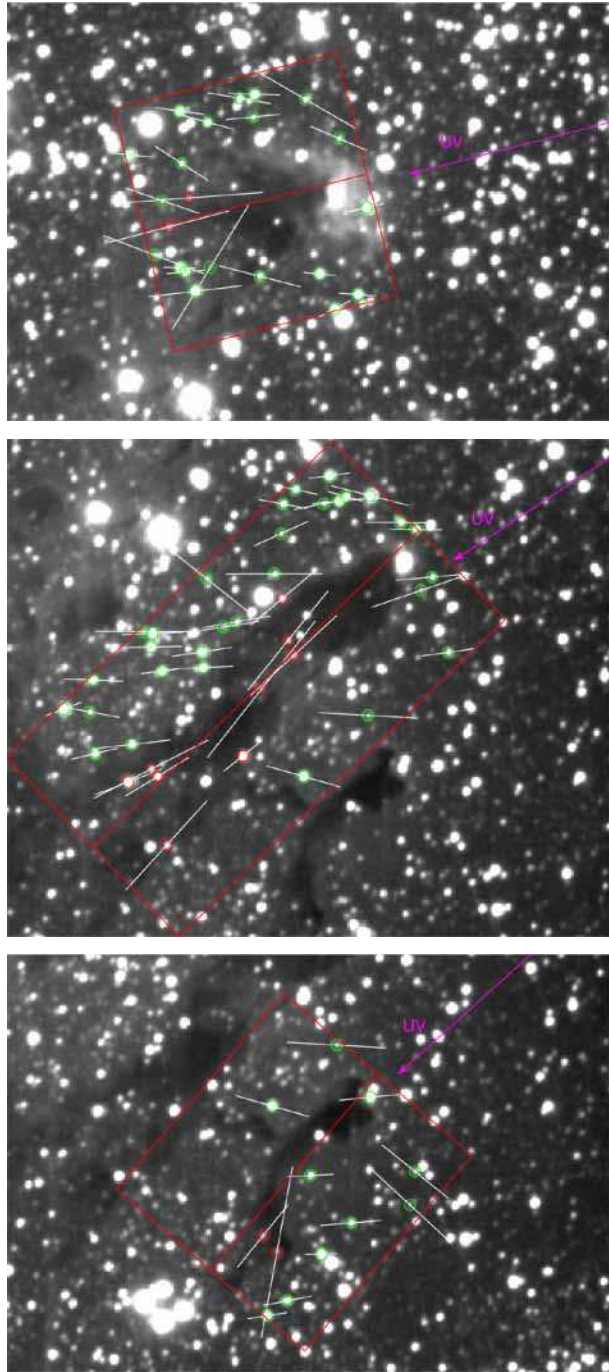


Fig. 9. H band images for position angle estimate in table 1. Sources within molecular clouds are marked by red circles and ones outside by green circles. The width of each image is $\sim 2.5'$. North is at the top, east to the left. See subsection 3.3.2 for more details.

ward the two nebulae illuminated by M16ES-1 and M16ES-2, at the tips of Pillars 1 and 2, which appear to be class I objects having circumstellar envelopes.

3. Our polarimetry results implies that M16ES-1 is an intermediate-mass object or lower-mass objects.
4. The mean position angle of global magnetic field is measured to be $\sim 80\text{--}90^\circ$, and seems to be consist with that of the previous optical polarimetry.
5. The alignment among the magnetic fields, axes and UV incident directions of Pillars 1–3, and the misalignment of the ambient/global magnetic fields to these directions suggest that the fields are affected by the dynamical impact of the UV radiation.

We thanks T. Nagata and S. Sato for helpful comments. This research was partly supported by MEXT, Grant-in-Aid Scientific Research on Priority Area, “Development of Extra-solar Planetary Science”, and by grants-in-aid from MEXT (Nos. 16077101 and 16077204). M. T. and R. K. acknowledge support by Grant-in-Aid (No. 16340061).

References

Andersen, M. et al. 2004, *A&A*, 414, 969
 Bertoldi 1989, *ApJ*, 349, 735
 Fischer, O., & Henning, T., & York, K. H. W. 1994, *A&A*, 284, 187
 Fukuda, N., Hanawa, T., & Sugitani, K. 2002, *ApJ*, 568, L127
 Healy, K. R., Hester, J. J., & Claussen, M. J. 2004, *ApJ*, 610, 835
 Hester, J. et al. 1996, *AJ*, 111, 2349
 Hester, J. J., Desch, S. J., & Healy, K. R., & Leshin, L. A. 2004, *Science*, 304, 1116
 Hester, J. J., & Desch, S. J., 2005, in *ASP Conf. Ser. 341, Chondrites and the Protoplanetary Disk*, ed. A. N. Krot, E. R. D. Scott & B. Reipurth (San Francisco: ASP)
 Kandori, R. et al. 2006, *Proc. SPIE*, 6269, 159
 Kessel-Deynet, O., & Burkert, A. 2003, *MNRAS*, 338, 545
 Lefloch, B., & Lazareff, B. 1994, *A&A*, 289, 559
 Martin, P. G. 1974, *ApJ*, 187, 461
 Messinger, D. W., Whittet, D. C. B., & Roberge, W. G. 1997, *ApJ*, 487, 314
 McCaughrean, M. J., & Andersen, M. 2001, ESO Press Release, (<http://www.eso.org/outreach/press-rel/pr-2001/phot-37-01.html>)
 McCaughrean, M. J., & Andersen, M. 2002, *A&A*, 389, 513
 Miao, J., White, G. J., Nelson, R., Thompson, M., & Morgan, L. 2006, *MNRAS*, 369, 143
 Nagashima, C. et al. 1999, in *Star Formation*, ed. T. Nakamoto (Nobeyama Radio Obs., Nobeyama), 397
 Nagayama, T. et al. 2003, *Proc. SPIE*, 4841, 459
 Orsatti, A. M., Vega, E. I., & Marraco, H. G. 2000, *A&AS*, 144, 195
 Orsatti, A. M., Vega, E. I., & Marraco, H. G. 2006, *AJ*, 132, 1783
 Pound, M. W. 1998, *ApJ*, 493, L113
 Sugitani, K., Tamura, M., & Ogura, K. 1995, *ApJ*, 455, L39
 Sugitani, K. et al. 2002, *ApJ*, 565, L25
 Tachibana, S., & Huss, G. R. 2003, *ApJ*, 588, L41
 Tachibana, S., Huss, G. R., Kita, N. T., Shimoda, G., & Morishita, Y. 2006, *ApJ*, 639, L87
 Tamura, M., Nagata, T., Sato, S., & Tanaka, M. 1987, *MNRAS*, 224, 413

Tamura, M., et al. 2006, ApJ, 649, L29
Tamura, M., et al. 2007, PASJ, in press
Thompson, R. I., Smith, B. A., & Hester, J. J. 2002, ApJ, 570,
749
Wardle, J. F. C., & Kronberg, P. P. 1974, ApJ, 194, 249
Warren-Smith, R. F., Draper, P. W., & Scarrott, S. M. 1987,
ApJ, 315, 500
White, G. J., et al. 1999, A&A, 342, 233
Whitney, B. A., & Hartmann, L. 1993, ApJ, 402, 605
Williams, R. J. R., Ward-Thompson, D., & Whitworth, A. P.
2001, MNRAS, 327, 788

Table 1. Position angles of the magnetic fields, pillar axes and directions from HD 168076 (O star).

Region		Magnetic Field (deg)	Pillar Axis (deg)	UV Incident Direction (deg)
Pillar 1	inside	99±5 (2)	~104	~104
	ambient	87±21 (19)
Pillar 2	inside	129±10 (9)	~134	~123
	ambient	91±13 (30)
Pillar 3	inside	155±14 (2)	~139	~132
	ambient	83±18 (10)
Global	...	84±22 (1227)

Note.— The position angles of magnetic fields were derived from *H* band data, and numbers of sample are given in parentheses.